



## Upscaling of Channel Systems in Two Dimensions Using Flow-Based Grids

X. H. WEN<sup>1</sup>, L. J. DURLOFSKY<sup>1, 2</sup> and M. G. EDWARDS<sup>3</sup>

<sup>1</sup>*ChevronTexaco Exploration and Production Technology Company, San Ramon, CA 94583-0719, U.S.A.*

<sup>2</sup>*Department of Petroleum Engineering, Stanford University, Stanford, CA 94305-2220, U.S.A.*

<sup>3</sup>*Department of Civil Engineering, University of Wales, Swansea, Swansea SA2 8PP, U.K.*

(Received: 25 June 2001; in final form: 2 July 2002)

**Abstract.** A methodology for the gridding and upscaling of geological systems characterized by channeling is presented. The overall approach entails the use of a flow-based gridding procedure for the generation of variably refined grids capable of resolving the channel geometry, a specialized full-tensor upscaling method to capture the effects of permeability connectivity, and the use of a flux-continuous finite volume method applicable to full tensor permeability fields and non-orthogonal grids. The gridding and upscaling procedures are described in detail and then applied to several two-dimensional systems. Significant improvement in the accuracy of the coarse scale models, relative to that obtained using uniform Cartesian coarse scale models, is achieved in all cases. It is shown that, for some systems, improvement results from the use of the flow-based grid, while in other cases the improvement is mainly due to the new upscaling method.

**Key words:** gridding, upscaling, streamlines, tensor permeability, heterogeneity, irregular geometry, effective permeability, reservoir simulation.

### 1. Introduction

Geological models of channel systems are often characterized by highly detailed geostatistical descriptions containing on the order of  $10^7$ – $10^8$  grid blocks. These models are generated using sophisticated geostatistical interpolation procedures (Damsleth *et al.*, 1992; Deutsch and Journel, 1998) constrained to honor measured well and seismic data. In addition, these fine scale descriptions reproduce the variability and correlation structure inherent in the actual formation, assuming the relevant geostatistical parameters can be estimated with reasonable accuracy. Models of this type are often far too detailed for use in routine flow simulators, so some type of coarsening or upscaling procedure must be applied. Though many such methods have been developed and used in a variety of settings, channel systems are particularly difficult to upscale accurately. This is because they generally display considerable geometric complexity coupled with very high and abrupt contrasts in rock properties (e.g. high permeability meandering channels immersed in a background of low permeability rock). King and Mansfield (1999) and King

*et al.* (1998) discuss in detail some of the inaccuracies that can result from the use of standard upscaling techniques with channel systems (for turbidite reservoirs) within a practical setting.

The purpose of this paper is to present methods appropriate for the upscaling of two-dimensional channel systems. The techniques developed here involve the use of flow-based information for the generation of coarse (structured and logically rectangular) curvilinear grids, the application of specialized procedures for the accurate calculation of upscaled permeability tensors, and the use of full tensor flux-continuous finite volume flow simulation. As we will show, the use of each of these techniques is important for the accurate modeling of channel systems on the coarse scale.

Flow-based gridding procedures have been developed by a variety of previous investigators within the context of reservoir simulation. Durlafsky *et al.* (1997) presented a nonuniform coarsening procedure for upscaling within a Cartesian grid framework. More general curvilinear grid generation procedures, based on the use of streamlines computed from a single-phase flow solution of the fine scale problem, have been implemented by a variety of researchers including Verma and Aziz (1997), Edwards *et al.* (1998), Portella and Hewett (2000), and Castellini *et al.* (2000). An alternate gridding procedure, based on the grouping of cells of similar permeability, was suggested by Garcia *et al.* (1992). These researchers introduced the concept of an 'elastic grid,' in which the grid is adjusted to minimize the variance of permeability within coarse grid cells. In subsequent work by Tran (1995) and Wen and Gomez-Hernandez (1996a, 1998), the general approach of Garcia *et al.* (1992) was combined with flow information to generate flow-based grids.

Many of these previous flow-based grid generation procedures use streamline information directly and may, as a result, provide grids with an extremely high concentration of grid lines in high flow regions. Like these earlier techniques, the flow-based grid generation method applied here uses streamline information, though we introduce a grid-smoothing step that provides more control over the local grid density. This capability introduces a considerable degree of flexibility into the overall gridding procedure.

The calculation of accurate coarse grid block permeability tensors (designated  $\mathbf{k}^*$ ) is another important aspect of the methodology presented here. A number of previous approaches for the calculation of  $\mathbf{k}^*$  have been presented; for detailed discussions of the various methods see Wen and Gomez-Hernandez (1996b) and Renard and de Marsily (1997). In this paper, we extend our recently developed methodology for the calculation of  $\mathbf{k}^*$  (Wen *et al.*, 2000, 2002) to approximately handle irregular (non-rectangular) grid blocks. This procedure entails the use of a 'border region' of fine grid cells around the coarse block for which  $\mathbf{k}^*$  is to be calculated. This technique was shown to be well suited to the calculation of equivalent permeability for rectangular grid blocks in systems containing oriented features of large correlation length, such as the channel systems considered here.

We note that King *et al.* (1998) presented an alternate procedure for the calculation of  $\mathbf{k}^*$  that used a different set of local boundary conditions as a means of capturing the effects of permeability connectivity.

The flow-based grids used in this study generally do not conform to the underlying fine grid; that is, the corner points of the coarse grid do not correspond to corner points of the fine geological grid. This introduces an additional complication into the calculation of the coarse block  $\mathbf{k}^*$ . Here we introduce a new treatment to address this issue.

This paper proceeds as follows. In Section 2, we present the governing equations for immiscible and unit mobility ratio displacements and motivate the need for upscaling. Our procedure for grid generation is discussed in Section 3. Next, in Section 4, we describe our technique for the calculation of coarse grid block permeability tensors. Extensive flow simulation results for channel systems are presented in Section 5. The significant advantages of the proposed methodology over simpler approaches are clearly demonstrated. In Section 6, we provide further discussion, followed by conclusions in Section 7.

## 2. Governing Equations and General Solution Procedure

Although our general interest is more toward problems involving two or more phases, our calculations in this paper mostly involve single-phase flow (though we do include a two-phase flow example). Because there is a close relationship between the single- and two-phase flow equations, and because we wish to motivate the need for upscaling in terms of two-phase flow calculations, we first discuss the more general two-phase flow equations. The displacing component is designated as water and the displaced component as oil. In the absence of gravity, compressibility, and capillary pressure effects, this system is described by

$$\nabla \cdot [\lambda(S)\mathbf{k}(\mathbf{x})\nabla p] = 0, \quad (1)$$

$$\frac{\partial S}{\partial t} + \nabla \cdot [\mathbf{u}f(S)] = 0, \quad (2)$$

where  $\mathbf{k}(\mathbf{x})$  is the spatially varying permeability tensor ( $\mathbf{x}$  designates spatial location),  $p$  is the pressure,  $S$  is the water saturation (volume fraction),  $\mathbf{u}$  is the Darcy velocity given by  $\mathbf{u} = -\lambda(S)\mathbf{k}(\mathbf{x})\nabla p$ , and the total mobility  $\lambda$  and the fractional flow  $f$  are defined as

$$\lambda(S) = \frac{k_{rw}}{\mu_w} + \frac{k_{ro}}{\mu_o}, \quad (3a)$$

$$f(S) = \frac{k_{rw}/\mu_w}{k_{rw}/\mu_w + k_{ro}/\mu_o}. \quad (3b)$$

Here,  $k_{rw}$  and  $k_{ro}$  are the relative permeabilities to water and oil and  $\mu_w$  and  $\mu_o$  are the phase viscosities. Porosity is assumed to be constant. The upscaled equations

are here taken to be of the same form as Equations (1)–(3) but with  $\mathbf{k}^*$  replacing  $\mathbf{k}$  in Equation (1) and Darcy's law.

The fine scale solution of Equations (1)–(3) can be very time consuming. At each time step, the coupled system must be solved; for an IMPES type procedure (implicit in pressure, explicit in saturation) this requires the solution of a linear system of size  $N_f$  (where  $N_f$  is the total number of fine grid blocks) at each time step. In addition, for a two-dimensional system in the  $x$ - $y$  coordinate system, the maximum stable time step for the explicit solution of Equation (2) scales with  $\Delta x_f$  and  $\Delta y_f$  (fine block sizes in the  $x$ - and  $y$ -directions). If the system is upscaled to  $N_c$  coarse grid blocks, the linear system is now of size  $N_c$  and the maximum stable time step size scales with the coarse block sizes  $\Delta x_c$  and  $\Delta y_c$ . Assuming uniform upscaling and a linear solver for which solution time scales linearly with the number of blocks, the coarse grid model will require a factor of about  $(N_f/N_c)^{3/2}$  less computation time than the fine model, for two-dimensional systems. For  $N_f/N_c = 25$  (upscaling by a factor of 5 in each dimension), the upscaled model will therefore only require about 1% of the CPU time of the fine grid model. Savings will in general be less if the model is upscaled nonuniformly, as the small grid blocks may limit the maximum stable time step. In any event, these savings will be achieved each time the model is run; that is, for each flow scenario that is simulated. Thus, it is clearly worth putting substantial effort into the gridding and upscaling procedures, particularly since these calculations need only be performed once in a pre-processing step.

The single phase, unit mobility ratio equations can be recovered from Equations (1)–(3) by setting  $k_{rw} = S$ ,  $k_{ro} = 1 - S$  and  $\mu_w = \mu_o$ , which results in  $\lambda = 1/\mu_w$  and  $f = S$ . In this case, there is no dependence on saturation in the pressure equation (1) or in the Darcy velocity and the saturation equation (2) reduces to a linear hyperbolic conservation law. This allows for the efficient solution of the governing equations, as the pressure and velocity fields do not require updating as the displacement progresses (i.e. the pressure equation need only be solved once). Also, the saturation equation can be solved efficiently in this case by integrating along streamlines. Using streamline integration to solve Equation (2), the coarse grid model will require a factor of about  $(N_f/N_c)$  less computation time than the fine model for each simulation performed.

Due to the similarity between the single- and two-phase flow equations, we expect that a coarse scale description (i.e. grid and coarse block  $\mathbf{k}^*$ ) that accurately represents a unit mobility system will be similarly applicable to the more general two-phase flow case. In addition, the flow-based grid generated through solution of a single-phase flow problem can also be expected to be applicable to two-phase flow problems since, for heterogeneity dominated problems, streamlines change relatively little during the course of the simulation (Hewett and Yamada, 1997). This assumption is implicit in many upscaling approaches, which use single phase, unit mobility ratio calculations in the grid determination step and as a 'diagnostic' to gauge the accuracy of a coarse scale reservoir description (see e.g. Durlofsky

*et al.*, 1997). The coarse scale description so determined is then used for multiphase flow calculations in a general reservoir simulator.

### 3. Flow-Based Grid Generation

In this section, we describe our method for the generation of a flow-based grid. The basic approach entails a single solution of the single-phase, steady-state pressure equation over the fine grid region. Though this solution does involve a fine grid calculation, it represents a fairly small computational cost relative to the solution of the two-phase system on either the fine or coarse scale (which, as discussed in §2, requires the solution of the pressure equation at every time step). The basic idea is to use streamlines to define the high flow paths and to introduce refinement in these areas. Although the grid is determined using flow-based information from a single fine grid solution, it is appropriate for use in a variety of related flow problems, as we shall show in the examples below. We note that the computational requirements for the grid generation method (essentially the time required for the single fine grid solution) are about the same as for existing procedures which generate nonuniformly coarsened Cartesian grids (Durlafsky *et al.*, 1997).

The fine grid permeability is in general a highly discontinuous, full tensor quantity. Specialized techniques are therefore required for the solution of the pressure equation (1). We solve Equation (1) using a flux-continuous finite volume method (Aavatsmark *et al.*, 1996; Edwards and Rogers, 1998; Lee *et al.*, 1998), which is well suited for problems involving full tensor permeabilities and grid non-orthogonality (i.e. non-rectangular grid blocks). For simplicity, we take the fine grid field to be defined on a Cartesian grid. The flow-based coarse grid models are, however, characterized by irregular quadrilateral grid blocks.

We generate the flow-based grid by first solving Equation (1) with  $\lambda = 1$  (in dimensionless terms) subject to  $p = 1$  on the left face ( $x = 0$ ),  $p = 0$  on the right face ( $x = L_x$ ) and no flow on the  $y = 0$  and  $y = L_y$  boundaries, where  $L_x$  and  $L_y$  denote the system lengths in the  $x$ - and  $y$ -directions. The linear system is solved using a multigrid method (Ruge and Stuben, 1987). Following this solution, streamlines can be generated through either a particle tracking technique or through the contouring of the streamfunction  $\Psi$  (we note that the particle tracking technique readily generalizes to three dimensions whereas the streamfunction technique does not). When the flow is driven by boundary conditions (rather than by wells), as is the case here, the streamfunction can be easily computed from the velocity in a post-processing step (see Durlafsky *et al.*, 1997 for details). Streamlines are then generated as lines of constant  $\Psi$ . Some number of these streamlines is then selected to provide one set of coordinate lines (the  $\xi$ -coordinates). Both the particle tracking and the streamfunction techniques were implemented in this study. In the examples below, we apply the streamfunction approach.

The other coordinate lines (the  $\eta$ -coordinates) can be obtained from iso-potentials (contours of constant pressure) or from streamlines generated from a

complementary flow problem. Another approach is to divide each  $\xi$ -coordinate line into a specified number of segments of equal arc length and to simply connect these segments. In the cases considered in this paper, the initial  $\eta$ -coordinate lines were determined through a weighted interpolation between isopotential curves and equal-arc length curves. In implementing this weighted interpolation, we computed the  $(x, y)$  locations of the intersections between the  $\xi$  and  $\eta$  coordinate lines using both isopotentials and equal arc lengths. The initial grid was then determined by weighting between these two results, with about 80% weighting on the isopotential  $(x, y)$  values and 20% weighting on the equal arc length values. The overall procedure is not overly sensitive to these weightings, though they were found to provide suitable initial grids.

Grids generated directly from streamlines introduce high levels of resolution in regions of high flow. This approach can result in grids with highly distorted cells and an overly high concentration of grid lines in high flow regions (and very few grid lines in lower flow regions). This can present difficulties if the grid is applied to problems that differ from that used to define the streamlines and can also lead to inaccuracy and very small time steps in finite volume solutions. To provide grids with more uniformity, we therefore introduce a grid-smoothing step, which we now describe.

The basic idea of our grid smoothing is to control the level of grid line concentration throughout the domain. The procedure we describe here is relatively simple, though more complex variants can be readily defined. Following the solution of Equation (1) on the fine scale in an  $x$ - $y$  coordinate system and the determination of the initial  $\xi$  and  $\eta$  coordinate lines, we determine the  $x$  and  $y$  locations of all of the grid line intersections. These intersections, designated  $x_{i,j}$  and  $y_{i,j}$ , provide the locations of the corner points of each coarse block.

The grid smoothing now entails a number of Laplacian-type iterations of the form:

$$x_{i,j}^{k+1} = (1 - \omega)x_{i,j}^k + \frac{1}{4}\omega(x_{i-1,j}^k + x_{i+1,j}^k + x_{i,j-1}^k + x_{i,j+1}^k), \quad (4a)$$

$$y_{i,j}^{k+1} = (1 - \omega)y_{i,j}^k + \frac{1}{4}\omega(y_{i-1,j}^k + y_{i+1,j}^k + y_{i,j-1}^k + y_{i,j+1}^k), \quad (4b)$$

where  $(x_{i,j}^k, y_{i,j}^k)$  with  $k = 1$  designates the initial grid,  $(x_{i,j}^{k+1}, y_{i,j}^{k+1})$  designates subsequent (smoothed) grids and  $\omega$  is a relaxation parameter ( $0 < \omega \leq 1$ ). The iterations were performed until relevant measures of grid quality, such as suitably defined maximum physical grid aspect ratio, maximum grid distortion, and maximum ratio of the spacing of adjacent nodes, were reduced to reasonable (user-prescribed) values. These grid quality measures can be computed from the local Jacobian components  $\mathbf{x}_\xi$  and  $\mathbf{x}_\eta$ . These quantities were reduced by up to an order of magnitude during the iteration process. There is of course a tradeoff between grid quality and the level of conformance of the grid to the streamlines; the intent

of the grid smoothing is to render the grid suitable for finite volume computations while maintaining a reasonable link to the flow information.

In the results presented here, we set  $\omega = 0.6$  and typically performed 2–5 iterations of Equations (4). Numerical experiments demonstrated that, for specified grid quality measures, the final grid was not very sensitive to the value of  $\omega$ . However, if smaller values of  $\omega$  were used, a greater number of iterations were required to achieve the specified grid quality measures. Equations (4) could be modified to provide for variable degrees of smoothing in different regions of the domain or to provide different types of smoothing in  $x$  and  $y$ . Though these variants could be implemented quite simply, they were explored only briefly in this work. We did not observe any numerical instabilities in iterating Equations (4), though it is possible that instability could occur if variable smoothing is performed and  $\omega$  is taken too large. Alternate grid smoothing procedures, such as those described by Knupp (1995, 1996), may also be suitable for this problem and will be explored in the future.

We note that unstructured (e.g. triangle-based) finite element methods could also be used for the grid construction and that these methods are inherently more flexible than the structured grid methods applied here. However, such grids are not compatible with many existing reservoir simulators. Thus, our emphasis here is on structured quadrilateral grids. We note that many of the techniques developed and applied here are, however, applicable to unstructured grids as well.

We now present an example illustrating this procedure. The permeability field for a channel system is depicted in Figure 1. The initial coordinate lines, generated as described above, are shown in Figure 2. The grid is clearly highly concentrated in some regions and very coarse in other regions. A more uniform grid, generated

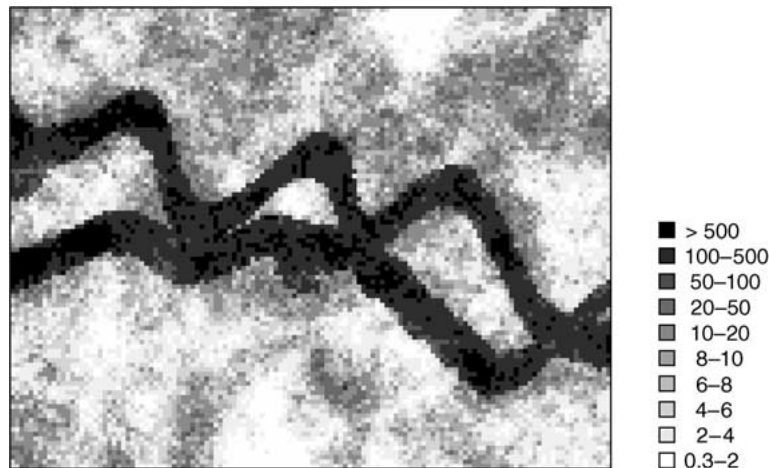


Figure 1. Permeability field for fluvial reservoir (from Mao and Journel, 1998). Permeability varies from 0.3 to 3225 md.

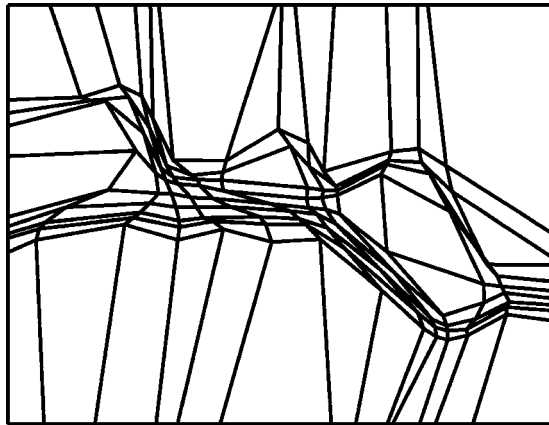


Figure 2. Initial flow-based grid for permeability field of Figure 1.

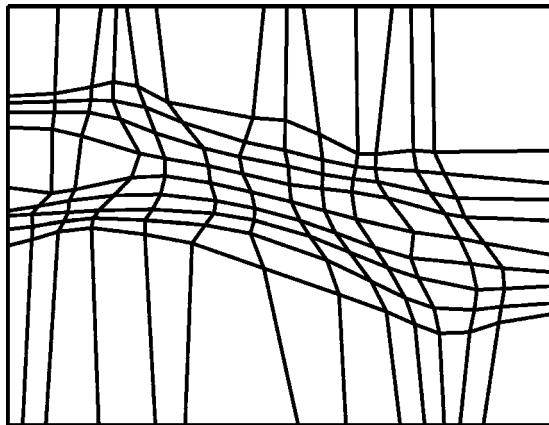


Figure 3. Final flow-based grid after smoothing.

using two smoothing iterations and  $\omega = 0.6$ , is displayed in Figure 3. The smoothed grid displays much less grid distortion, with distortion quantified in terms of the maximum angle in any of the quadrilaterals. This grid is now well suited for flow calculations, as will be illustrated in Section 5 below.

#### 4. Calculation of Coarse Grid Permeability Tensors

Our basic procedure for the calculation of the coarse block permeability tensor  $\mathbf{k}^*$  entails the solution of a local problem subject to periodic boundary conditions (Durlafsky, 1991; Wen *et al.*, 2000, 2002). Here, we will present the basic approach and then discuss extensions to handle irregularly shaped (non-rectangular) coarse blocks and coarse blocks that do not conform to the underlying fine grid. The

procedure requires the solution of the single phase pressure equation over a fine grid region corresponding to the coarse block for which  $\mathbf{k}^*$  is to be calculated. The solution region may additionally contain fine grid permeability data bordering the target coarse block, as discussed below.

In our local solution of the fine grid permeability field, we impose periodic boundary conditions coupled with a large scale gradient in pressure. These boundary conditions have several positive features, including a high degree of robustness and the generation of symmetric, positive definite  $\mathbf{k}^*$ . However, as is the case with other boundary specifications, they are not generally able to capture effects due to large scale permeability connectivity at arbitrary orientations, which can be very important in models of channel systems.

In Wen *et al.* (2000, 2002), we demonstrated that the use of bordering rings of fine grid cells can better capture the effects of oriented large scale permeability connectivity on Cartesian grids. Because they capture these larger scale effects, the use of border regions leads to coarse scale models that are better able to predict the breakthrough of injected fluid. The basic approach for a rectangular grid is illustrated in Figure 4. In the figure, the finer grid lines correspond to the fine grid and the heavier lines to the coarse grid. Here we include the bordering fine grid region corresponding to a single ring of coarse blocks around the target coarse block (shaded). The number of border ‘rings’ in this case, designated  $r$ , is therefore 1, which is usually sufficient. We note that border regions similar to those used here were previously applied, in a variety of contexts, by several investigators (e.g. Holden and Lia, 1992; Gomez-Hernandez and Journel, 1994; Hou and Wu, 1997; Efendiev, 1999). However, in this paper the emphasis is on irregular quadrilateral grids coupled with oriented, geometrically complex permeability fields, resulting in potentially strong full tensor effects on the coarse scale.

The procedure to calculate  $\mathbf{k}^*$  is as follows. We solve Equation (1) with  $\lambda = 1$ , subject to periodic boundary conditions, over the domain of Figure 4 (target coarse block plus border regions) to obtain a local fine grid solution of  $p$  and  $\mathbf{u}$ . Two such

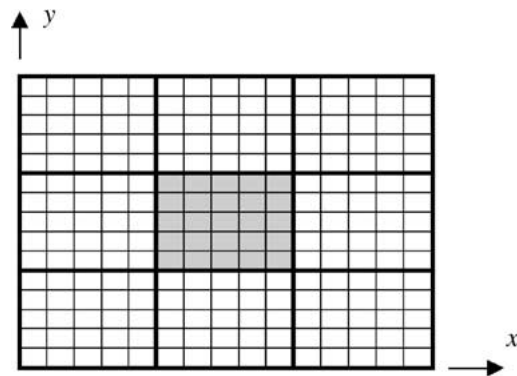


Figure 4. Schematic illustrating use of border regions ( $r = 1$ ) for rectangular grid.

solutions are required, with two linearly independent large scale pressure gradients specified. The specific boundary conditions are as follows:

$$p(0, y) = p(l_x, y) + G_x l_x, \quad (5a)$$

$$p(x, 0) = p(x, l_y) + G_y l_y, \quad (5b)$$

$$u_x(0, y) = u_x(l_x, y), \quad (5c)$$

$$u_y(x, 0) = u_y(x, l_y), \quad (5d)$$

where  $G_x$  and  $G_y$  designate the components of the large scale pressure gradient and  $l_x$  and  $l_y$  are the lengths of the domain in Figure 4 in the  $x$ - and  $y$ -directions. In the first solution of Equation (1) subject to (5) we specify  $G_x = 1$  and  $G_y = 0$ ; in the second solution we set  $G_x = 0$  and  $G_y = 1$ . A value for pressure must also be specified at one point in the domain.

Using the pressure field, we compute the area-averaged velocity and pressure gradient, designated  $\langle \mathbf{u} \rangle$  and  $\langle \nabla p \rangle$ , over the target coarse block (shaded region in Figure 4). The four components of the coarse grid block permeability are then computed from these two flow solutions using

$$\langle \mathbf{u} \rangle = -\mathbf{k}^* \cdot \langle \nabla p \rangle. \quad (6)$$

Due to the use of the border regions, the permeability computed for the target cell is in general not symmetric; symmetry is imposed by simply averaging the two off-diagonal terms ( $k_{xy}^*$  and  $k_{yx}^*$ ). In some rare cases the resulting block  $\mathbf{k}^*$  computed in this way is not positive definite. In such cases we simply solve the local problem over the coarse cell with no border region (i.e. we set  $r = 0$ ).

Additional complications, not addressed by Wen *et al.* (2000, 2002), arise when the coarse block is non-rectangular and does not conform to the underlying fine grid, as will occur when a flow-based grid as described above is used. This case is illustrated in Figure 5. The fine grid is again designated by the finer lines and the coarse grid (nine irregular quadrilaterals) by the heavier lines. The target coarse block is the central block; the other eight blocks represent the surrounding region ( $r = 1$  in this case). We define the local solution domain as the rectangular region containing the coarse cell corner points and a number of additional fine grid cells corresponding to the dimensions of the target coarse cell. Specifically, for the case where the coarse cell corner points fall within a  $6 \times 4$  rectangle of fine cells (as in Figure 5), the local problem will be expanded by 6 cells in the  $-x$  and  $+x$  directions and by 4 cells in the  $-y$  and  $+y$  directions (for  $r = 1$ ). In this case, the local solution will contain  $18 \times 12$  fine cells (the entire domain shown in the figure).

We solve Equation (1) subject to (5) over this region. The quantities  $\langle \mathbf{u} \rangle$  and  $\langle \nabla p \rangle$  are computed only over the fine grid blocks whose centers fall within the

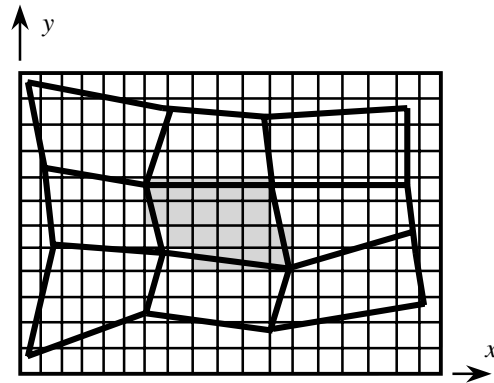


Figure 5. Schematic illustrating use of border regions ( $r = 1$ ) for general curvilinear grid.

target coarse block (these fine blocks are shaded in the figure) and Equation (6) is then applied to compute  $\mathbf{k}^*$ . Though this procedure handles geometric effects in an approximate manner, it appears to be of reasonable accuracy for the problems considered here. A more involved approach, in which the coarse grid geometry is resolved exactly using a triangle-based finite element method, represents another alternative for the calculation of  $\mathbf{k}^*$  (see He *et al.*, 2002). We plan to compare the results from these two procedures in subsequent work.

The algorithm described here for computing coarse scale permeability requires the solution of the local (target cell plus border region) fine scale pressure equation for each coarse grid block. In the examples below, we upscale the fine model by factors ranging from 8 to 100 (in two dimensions). Consider a representative case, where the fine grid problem is of dimensions  $100 \times 100$  and we uniformly upscale to a coarse scale description of dimensions  $20 \times 20$  using  $r = 1$ . For this example, 400 local problems of dimension  $15 \times 15$  (except near the boundaries), are solved to determine the grid block  $\mathbf{k}^*$ . In cases where we upscale by a factor of 10, the local problems will be of dimension  $30 \times 30$  (for  $r = 1$ ). We solve these linear systems in all cases using a multigrid method (Ruge and Stuben, 1987).

## 5. Simulation Results

We now present a series of simulation results for three types of systems. We quantify the accuracy of the coarse scale results through comparisons with the reference fine grid results. Results using both flow-based and uniform Cartesian grids are presented. We do not consider nonuniform Cartesian grids of the type generated by Durlofsky *et al.* (1997). Such grids would be expected to perform better than the uniform Cartesian grids but not as well as the flow-based grids. This is because coarse rectangular grids are not as well suited for the geometrically complex systems considered here as are flow-based grids.

The flow quantities we compare are the global effective permeability (or total flow rate through the system), for a given set of pressure boundary conditions, and the fractional flow of displaced fluid (oil) at the production boundary as a function of dimensionless time (pore volumes injected or PVI). We now describe how these quantities are computed. From the solution of Equation (1) subject to pressure and no-flow boundary conditions, we can compute the total flow rate through the system  $Q$ . If pressure boundary conditions are specified at  $x = 0$  and  $x = L_x$ , we compute the global effective permeability in the  $x$ -direction  $K_{g,x}$  as

$$K_{g,x} = \frac{QL_x}{L_y \Delta p}, \quad (7)$$

where  $\Delta p$  is the difference in pressure between  $x = 0$  and  $x = L_x$ . For global flow in the  $y$ -direction, a similar expression for  $K_{g,y}$  can be obtained.

Comparisons between  $K_g$  for fine and coarse models provide a measure of the accuracy of the upscaling techniques for global flow quantities. To quantify their accuracy for more detailed effects, such as fluid breakthrough, we compute the fractional flow of oil (oil cut), designated  $F_o$ , as a function of PVI. For the unit mobility ratio case ( $f = S$ ), this can be readily computed from Equation (2), with  $\mathbf{u}$  determined from the solution of Equation (1). We compute  $F_o$  via an integration of Equation (2) along streamlines. In the case of non-rectangular grid blocks, as will result when flow-based grids are used, we use the method of Prevost *et al.* (2002) for an accurate integration of Equation (2).

### 5.1. TWO DOMINANT CHANNELS

We now consider our first example case. The permeability field is as shown in Figure 1 above. The fine grid is  $130 \times 100$  (NX  $\times$  NY). This single layer model is the bottom layer of the three-dimensional Stanford V data set, a geostatistical representation of a fluvial channel reservoir (Mao and Journel, 1998). The physical dimensions of this system are 1300 ft  $\times$  1000 ft, with uniform cell size of 10 ft  $\times$  10 ft. Channels span the system in the  $x$ -direction and are of typical width of about 50–100 ft. We note that, in our upscaled model, we wish to resolve effects on the scale of the channel width. The flow-based grid, of dimensions  $13 \times 10$ , is shown in Figure 3. The system in this case contains two dominant channels, of similar orientation. We would therefore expect this model to be well suited for flow-based gridding.

Flow results, in terms of  $F_o$  versus PVI, are shown in Figure 6. Flow in this case is in the  $x$ -direction and is driven by boundary conditions of the same form as those used to develop the initial streamlines for the generation of the grid. Water is injected along the left-hand side boundary. In the figure, the solid line represents the fine scale result, the dashed line the coarse scale result using the flow-based grid with  $r = 1$ , the dot-dash line the coarse scale result using the flow-based grid with  $r = 0$ , and the dotted line the result using a uniform coarse grid (also of dimensions

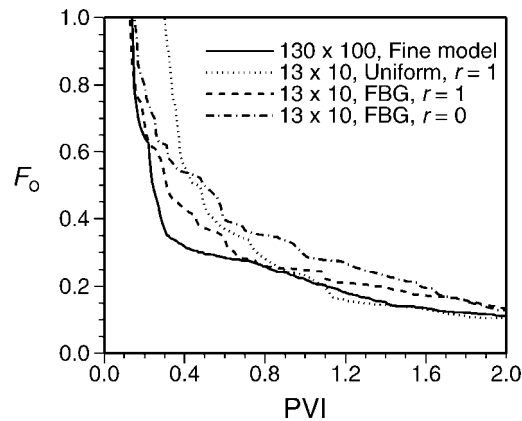


Figure 6. Fractional flow results for global flow in the  $x$ -direction in fluvial reservoir.

$13 \times 10$ ) with  $r = 1$ . Results with a uniform grid and  $r = 0$  are very close to those with  $r = 1$  and are therefore not shown. The results with the flow-based grid are clearly more accurate, relative to the reference fine grid results, than those using the uniform grid, particularly in their prediction of breakthrough and early time behavior. In addition, the flow-based grid results with  $r = 1$  are noticeably more accurate than those with  $r = 0$ . This illustrates the importance of both the coarse grid structure and the way in which the coarse grid  $\mathbf{k}^*$  is calculated.

The coarse scale results for total flow rate through the system ( $K_{g,x}$ ) are as follows. For the fine grid  $K_{g,x} = 44.2$ ; for the uniform coarse grid with  $r = 1$ ,  $K_{g,x} = 26.3$  (an error of 40%) and for the flow-based grid with  $r = 1$ ,  $K_{g,x} = 36.7$  (error of 17%). These errors increase if we use  $r = 0$  instead of  $r = 1$  (to 54 and 36% for the uniform and flow-based grids, respectively). These errors decrease, by contrast, as the coarse grid is refined. For example, we computed results on  $20 \times 15$  uniform and flow-based grids ( $r = 1$  in both cases) and obtained results for  $K_{g,x}$  of 30.8 and 40.0, respectively. Thus, at this level of upscaling, the flow-based grid provides results for  $K_{g,x}$  that differ by less than 10% from the fine grid results. The results for fractional flow of oil are also more accurate for the  $20 \times 15$  models.

## 5.2. INTERSECTING CHANNELS

The next example involves a single layer taken from a three-dimensional description of a North Sea reservoir. This system is layer 61 of the reservoir considered in the SPE comparative solution project on upscaling (Christie and Blunt, 2001). This portion of the reservoir, shown in Figure 7, corresponds to the Upper Ness formation, a fluvial depositional environment. The fine grid in this case is  $220 \times 60$ . The physical dimensions of this system are 4400 ft  $\times$  1200 ft, with uniform fine cell size of 20 ft  $\times$  20 ft. The accuracy of the coarse scale model in this case is quite sensitive to the grid dimensions. We therefore upscale this model by only a factor of 8, to  $55 \times 30$ . The flow-based coarse grid is shown in Figure 8. Due to the highly

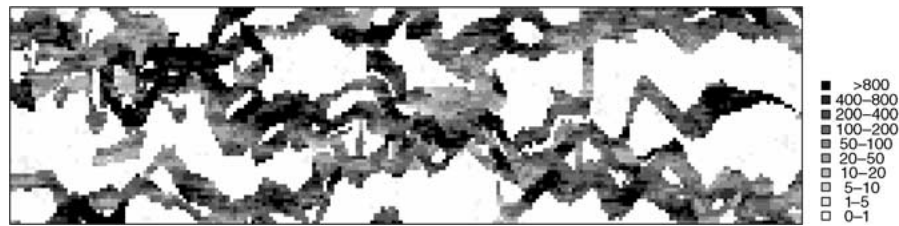


Figure 7. Permeability field for Upper Ness reservoir (from Christie and Blunt, 2001). Permeability varies from 0.001 to 20 000 md.

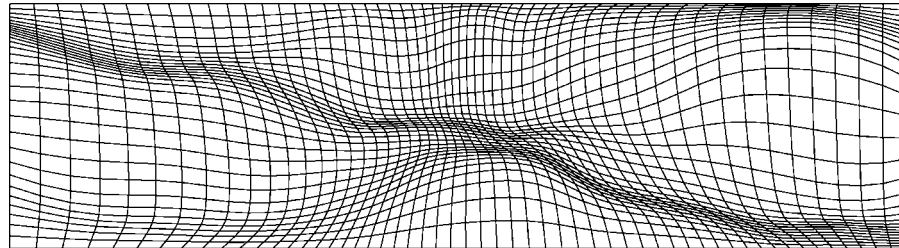


Figure 8. Flow-based grid (after smoothing) for permeability field of Figure 7.

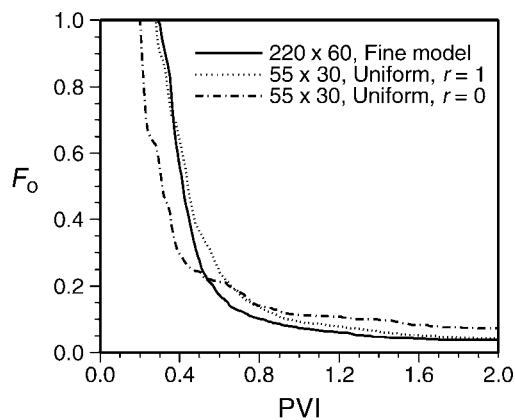


Figure 9. Fractional flow results for global flow in the  $x$ -direction in Upper Ness reservoir (uniform coarse grid).

variable nature of the channel geometry, the grid is not able to resolve the channels as accurately as in the previous example (cf. Figure 3). Boundary conditions are the same as described previously.

In this case, the upscaled models are more sensitive to the calculation of the coarse block  $\mathbf{k}^*$  than to the grid structure. This is illustrated in the following figures. Displayed in Figure 9 are results for  $F_o$  versus PVI for flow in the  $x$ -direction for a uniform coarse grid (of dimensions  $55 \times 30$ ). The solid line corresponds to the fine grid result, the dotted line to the coarse grid result using  $r = 1$  and the dot-dash line to the coarse grid result using  $r = 0$ . The model with  $r = 1$  clearly displays better accuracy, relative to the fine grid result, than does the model with  $r = 0$ , over

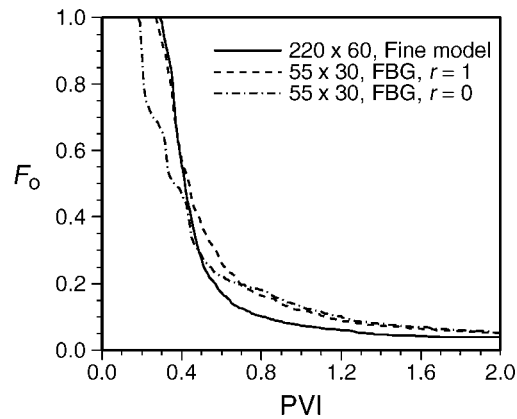


Figure 10. Fractional flow results for global flow in the  $x$ -direction in Upper Ness reservoir (flow-based coarse grid).

essentially the entire course of the simulation. This is also the case if we compare results for  $K_{g,x}$ . Specifically, the fine model gives  $K_{g,x} = 52.4$ ; for the uniform coarse grid with  $r = 0$ ,  $K_{g,x} = 29.0$  (an error of 45%) and for the uniform coarse grid with  $r = 1$ ,  $K_{g,x} = 38.9$  (error of 26%).

Results for fractional flow using the  $55 \times 30$  flow-based grid are shown in Figure 10. Again, the results with  $r = 1$  are more accurate than those using  $r = 0$ . Interestingly, the flow-based grid results in this case are very similar to those using the uniform coarse grid for both  $r = 1$  and  $r = 0$  (compare Figures 9 and 10). However, results for  $K_{g,x}$  are slightly better using the flow-based grid than using the uniform grid. Specifically, for  $r = 1$ ,  $K_{g,x} = 44.0$  using the flow-based grid (an error of 16%), compared to  $K_{g,x} = 38.9$  (error of 26%) for the uniform grid. For  $r = 0$ , the flow-based grid gives the same value for  $K_{g,x}$  as does the uniform grid (i.e.  $K_{g,x} = 29.0$ , an error of 45%).

Ideally, the upscaled models we generate should be applicable for boundary conditions other than those used in the grid generation step. We next display results for two different boundary conditions. In the first case, flow is from the upper left of the region to the lower right. This is accomplished by specifying  $p = 1$  over  $x = 0$ ,  $0.9L_y < y < L_y$  and  $p = 0$  over  $x = L_x$ ,  $0 < y < 0.1L_y$ . Results for fractional flow using the  $55 \times 30$  flow-based and uniform grids are shown in Figure 11. Both results are in reasonably close agreement with the fine grid results, though the flow-based grid does provide a slight improvement in accuracy. Errors in total flow rate are, however, significant in this case: the flow-based grid shows an error of 35% while the uniform grid displays an error of 57%. Results for flow from the lower left to the upper right are shown in Figure 12. Again, both results agree closely with the fine grid result. Total flow rates are more accurate in this case, with the flow-based grid giving an error of 17% and the uniform grid an error of 24%.

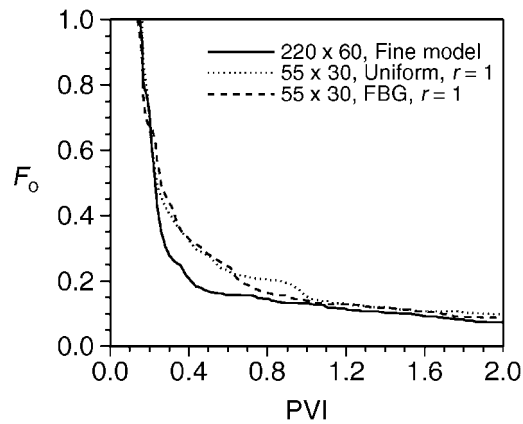


Figure 11. Fractional flow results for global flow from upper left to lower right in Upper Ness reservoir.

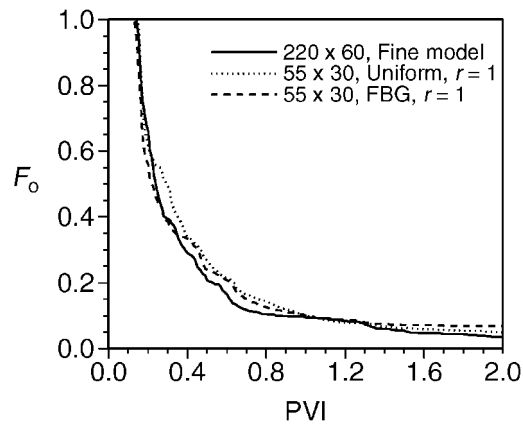


Figure 12. Fractional flow results for global flow from lower left to upper right in Upper Ness reservoir.

### 5.3. ORIENTED SYSTEM

Our next example involves a permeability field with oriented layers, generated using Gaussian sequential simulation (Deutsch and Journel, 1998). Though not technically a channel system, this example may represent a limiting case; that is, a system of parallel channels oriented at an angle to the system boundaries. This system is of additional interest since permeability on the fine grid is a full tensor quantity.

The permeability field is of dimension  $100 \times 100$  and displays layering (and principal axes of permeability) oriented at an angle  $\theta$  of  $30^\circ$  relative to the  $x$ -axis. The correlation length along the direction of the layering is  $0.8L$  while the correlation length normal to the layering is  $0.04L$ , where  $L = L_x = L_y$  is the length of a side of the (square) domain. Permeability is log-normally distributed, with the variance of  $\log k$  equal to 4. In each fine scale block we set  $k_2 = 0.1k_1$ ,

where  $k_1$  is the principal value of permeability in the direction along the layering and  $k_2$  is the principal value of permeability in the direction across the layering. The permeability in the  $x$ - $y$  coordinate system is therefore a full tensor quantity, which can be determined from  $k_1$  and  $k_2$  in each block and  $\theta$  via

$$\mathbf{k}(x, y) = \begin{bmatrix} k_1 \cos^2 \theta + k_2 \sin^2 \theta & (k_1 - k_2) \sin \theta \cos \theta \\ (k_1 - k_2) \sin \theta \cos \theta & k_1 \sin^2 \theta + k_2 \cos^2 \theta \end{bmatrix}, \quad (8)$$

where  $\theta = 30^\circ$ . The permeability field is shown in Figure 13 ( $\log(k_1)$  is the scalar quantity actually displayed in the figure). The flow-based grid for this permeability field, of dimensions  $20 \times 20$ , is shown in Figure 14.

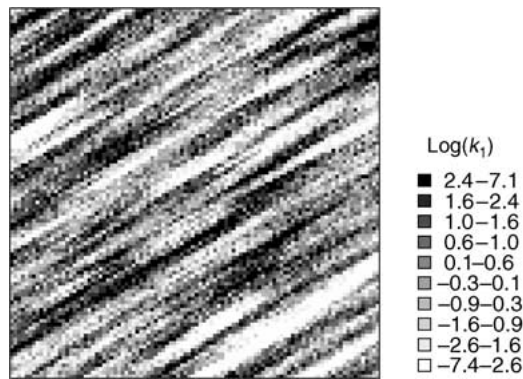


Figure 13. Permeability field with layering oriented at  $30^\circ$ . Permeability component  $k_1$  varies from 0.0006 to 1212 md.

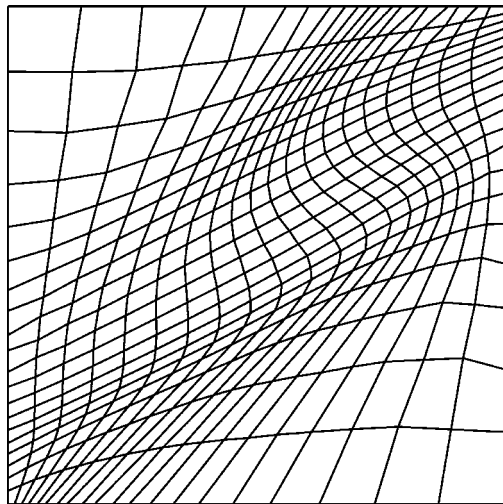


Figure 14. Flow-based grid (after smoothing) for permeability field of Figure 13.

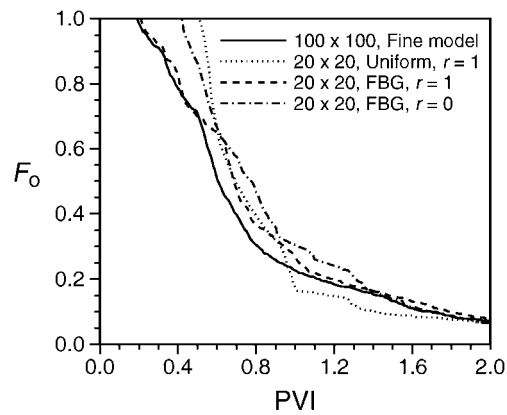


Figure 15. Fractional flow results for global flow in the  $x$ -direction in oriented system.

Flow results, in terms of  $F_o$  versus PVI, are shown in Figure 15. Flow in this case is in the  $x$ -direction and is driven by boundary conditions of the same form as those used to develop the initial streamlines. The flow-based grid result (with  $r = 1$ ) is clearly in close agreement with the fine grid result. This is in contrast to the uniform grid result (again with  $r = 1$ ) which shows noticeable differences, particularly around the time of water breakthrough. Differences between the flow-based grid results with  $r = 1$  and those with  $r = 0$  are also evident, illustrating the importance of both the grid structure and the way in which coarse scale permeability is calculated. For the uniform grid, there was little difference between the  $r = 1$  and  $r = 0$  results, though the  $r = 1$  results did show a slightly earlier breakthrough (0.47 PVI for  $r = 1$  compared to 0.51 PVI for  $r = 0$ ).

For total flow quantities, the fine model gives  $K_{g,x} = 0.64$ ; the uniform coarse grid with  $r = 1$  gives  $K_{g,x} = 0.50$  (an error of 22%) and the flow-based coarse grid with  $r = 1$  gives  $K_{g,x} = 0.61$  (error of 5%). For  $r = 0$ , the flow-based grid gives a result for  $K_{g,x}$  that is in error by 25%, while the uniform grid gives a result in error by 34%. The flow-based grid with  $r = 1$  is clearly preferable for this example.

We next display results for flows driven by different boundary conditions. In the first case, flow is from the bottom to top ( $p = 1$  along  $y = 0$ ,  $p = 0$  along  $y = L_y$ , no-flow along  $x = 0$  and  $x = L_x$ ). Both the flow-based and uniform grids provide comparable results for this problem, as shown in Figure 16. Though these results are reasonably accurate, some error in the prediction of breakthrough time is apparent. Both models also provide values for  $K_{g,y}$  that are within 8% of the fine grid solution. We note that the flow-based grid is in a sense least suited for this case, since flow is essentially along the grid isopotentials rather than along streamlines. Nonetheless, the flow-based grid does provide reasonable results, illustrating the robustness of the smoothed grid.

Results for flow from the lower left corner to the upper right corner, driven as described above, are shown in Figure 17. Flow in this case is along the high permeability direction ( $k_1$ ) of the layering. Here, the flow-based grid is seen to

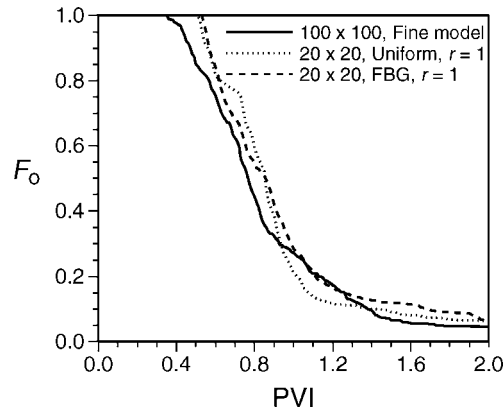


Figure 16. Fractional flow results for global flow in the  $y$ -direction in oriented system

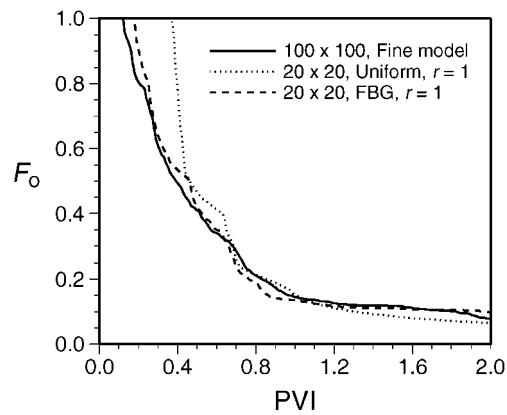


Figure 17. Fractional flow results for global flow from lower left to upper right in oriented system.

provide far more accurate results than the uniform grid, most notably at early times. The flow-based grid also gives better results for the total flow rate: the error using the uniform grid is 22%, while for the flow-based grid it is only 10%.

#### 5.4. TWO-PHASE FLOW THROUGH ORIENTED SYSTEM

Our final calculations are for two-phase flow through the oriented system considered above. Here we take  $\mu_o/\mu_w = 10$  and set  $k_{rw} = S^2$  and  $k_{ro} = (1 - S)^2$ . These functions are the same on the fine and coarse scales. In this case the mobility  $\lambda(S)$  in Equation (1) and thus the Darcy velocity  $\mathbf{u}$  in Equation (2) varies with time. Therefore, Equation (1) must now be solved at every time step. The coupled equations (1) and (2) are solved using an IMPES procedure with a variable time step based on the flow velocity and grid block size. We used a relatively simple

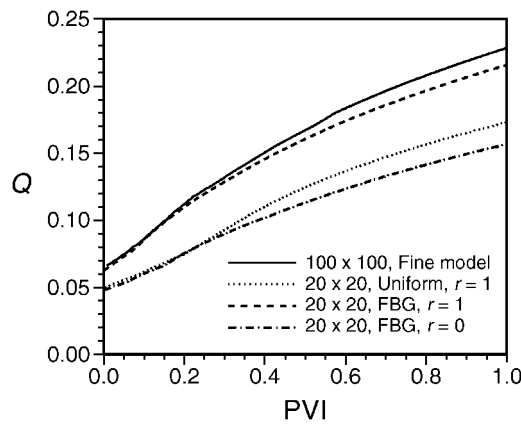


Figure 18. Two-phase flow results for oriented system: total flow rate for global flow in the  $x$ -direction.

procedure for time step selection; the timings for all of the models could be improved through use of a more sophisticated approach. The linear system resulting from Equation (1) is solved using a preconditioned GMRES (generalized minimum residual) type of iterative technique (Wallis *et al.*, 1985). Equation (2) is solved using a finite volume procedure.

We specify fixed pressures at the left and right edges of the model and fix the inlet saturation at  $S = 1$ . Fine, uniformly coarsened (with  $r = 1$ ) and coarsened models using the flow-based grid (with both  $r = 0$  and  $r = 1$ ) were simulated. Because the flow rate through the system varies in time, we cannot simply compare the  $K_{g,x}$  as computed from Equation (7) for the various models. Rather, we compare the total flow rate through the system ( $Q$ ) versus PVI for the different models. Fine and coarse scale flow results for  $Q$  are shown in Figure 18. From the figure, it is clear that the results for the flow-based grid with  $r = 1$  are in much closer agreement with the fine grid results than are the results from the uniformly coarsened model with  $r = 1$  or from the flow-based grid with  $r = 0$ . These results are consistent with the results for  $K_{g,x}$  for single phase flow presented above.

Figure 19 displays results for fractional flow for the two-phase system. The flow-based grid result with  $r = 1$  is again in reasonably close agreement with the fine grid result, while the predictions for the uniform grid with  $r = 1$  and the flow-based grid with  $r = 0$  show larger differences. These results clearly demonstrate that the grids generated by solving a global single phase flow problem are still appropriate for use in two-phase flow problems. This is consistent with previous findings in the context of nonuniform coarsening (Durlafsky *et al.*, 1997) and is also consistent with the observation that, in heterogeneity dominated problems, the variation of the streamlines with time is relatively small (Hewett and Yamada, 1997).

The upscaled model requires significantly less computational time than the fine grid model for this case. Specifically, the fine grid model required a factor of

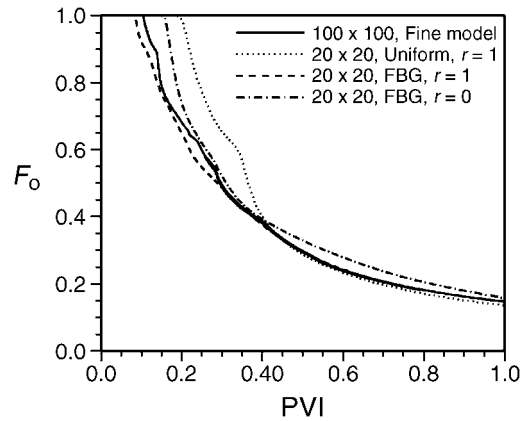


Figure 19. Two-phase flow results for oriented system: fractional flow of oil for global flow in the  $x$ -direction.

60 times more computation time than the coarsened flow-based grid model. This savings is very significant and is along the lines of that estimated in Section 2. It is important to note in addition that these savings will be achieved each time the model is run. We note finally that the grid generation and grid block permeability calculation required about 0.4% of the fine grid simulation time. These calculations need only be performed once, and thus represent a small overhead, particularly when many different coarse grid simulations are to be run.

## 6. Discussion

In this paper, we presented a new methodology for the gridding and upscaling of channel systems in two dimensions. The strategy contains three essential features: a flow-based gridding procedure, a specialized procedure for computing the upscaled cell permeability tensor, and the use of a flux-continuous finite volume method applicable to full tensor permeability fields and non-orthogonal grids. The flow-based gridding procedure together with the grid-smoothing algorithm provides a robust, graded mesh with higher concentrations of grid nodes in high flow regions. Through the use of border regions, the upscaling method captures the effects of the neighboring permeability field on the target cell and reduces the effects of the boundary conditions on the computed  $\mathbf{k}^*$ . The flow-based grid generation and upscaling procedures require only slightly more computation time than existing nonuniform coarsening procedures (e.g. Durlofsky *et al.*, 1997) but are better suited for the geometrically complex systems considered in this paper.

For any particular problem involving a channel system, the three components of the general methodology will probably not be equally important. In some cases, such as those containing a single dominant channel or multiple channels with

similar orientations, it is reasonable to expect that the use of a flow-based grid will lead to improved results over those attainable with uniform Cartesian grids. The impact of the flow-based grid was clearly illustrated in the first and third example cases above (involving two dominant channels and an oriented system). In models for which there is not a single dominant feature or a uniform orientation of features, the impact of the grid is expected to be less. This was illustrated in the second example above (intersecting channels). In this case, significant improvement in the coarse model was achieved through use of a border region in the  $\mathbf{k}^*$  calculation. Though our emphasis in this paper is on channel systems, the gridding and upscaling procedures presented here are clearly applicable to a wide variety of geological models.

Another important aspect of any gridding and upscaling procedure is the use of flow-based diagnostics to assess the quality of the upscaled model. Single-phase flow and unit mobility ratio displacement calculations, such as those presented here, are particularly well suited for this purpose (see e.g. Durlofsky *et al.*, 1997). These calculations give a clear gauge of the appropriate degree of upscaling for a particular problem. The applicability of such diagnostics was clearly illustrated in the last example, where it was demonstrated that the coarse scale grid and  $\mathbf{k}^*$  that provided accurate unit mobility ratio displacement results also provided accurate two-phase flow results. These diagnostics are relatively inexpensive computationally within the context of flow-based gridding procedures since fine scale flows are already computed in the grid generation step. The ability to perform an efficient and accurate assessment of the coarse scale model represents a significant advantage for flow-based gridding techniques over other grid generation procedures that are not based on fine scale flow solutions.

## 7. Conclusions

The following main conclusions can be drawn from this work:

- A general upscaling and flow-based grid generation methodology, appropriate for channelized and other geologically complex systems, was developed and applied. The method entails the use of smoothed streamline-based grids, the accurate calculation of upscaled permeability on general quadrilateral cells, and the use of full tensor permeabilities in all flow calculations.
- The procedure was shown to provide considerably more accurate coarse scale models than those generated using standard techniques. Enhanced accuracy was observed for total flow rate and the breakthrough of injected fluid in a number of cases.
- The overall methodology is computationally efficient and does not require significantly more work than existing nonuniform coarsening approaches.

## Acknowledgements

We are grateful to Seong Lee (ChevronTexaco EPTC) for providing the flux-continuous finite volume code used in this work, to Mathieu Prevost (Stanford University) for useful discussions regarding streamline methods with irregular quadrilateral cells, and to Chuanping He (Stanford University) for providing us with results on the sensitivities of the flow-based grids to the grid generation parameters.

## References

- Aavatsmark, I., Barkve, T., Boe, O. and Mannseth, T.: 1996, Discretization on non-orthogonal, quadrilateral grids for inhomogeneous, anisotropic media, *J. Comp. Phys.* **127**, 2–14.
- Castellini, A., Edwards, M. G. and Durlofsky, L. J.: 2000, Flow based modules for grid generation in two and three dimensions, In: *Proceedings of the 7th European Conference on the Mathematics of Oil Recovery*, Baveno, Italy, September 5–8.
- Christie, M. A. and Blunt, M. J.: 2001, Tenth SPE Comparative Solution Project: a comparison of upscaling techniques, paper SPE 66599 presented at the SPE Reservoir Simulation Symposium, Houston, February 11–14.
- Damsleth, E., Tjolsen, C. B., Omre, H. and Haldorsen, H. H.: 1992, A two-stage stochastic model applied to a North Sea reservoir, *J. Pet. Tech.* **22**, 402.
- Deutsch, C. V. and Journel, A. G.: 1998, *GSLIB: Geostatistical Software Library and User's Guide*, 2nd edn., Oxford University Press, New York.
- Durlofsky, L. J.: 1991, Numerical calculation of equivalent grid block permeability tensors for heterogeneous porous media, *Water Resour. Res.* **27**, 699–708.
- Durlofsky, L. J., Jones, R. C. and Milliken, W. J.: 1997, A nonuniform coarsening approach for the scale-up of displacement processes in heterogeneous porous media, *Adv. Water Resour.* **20**, 335–347.
- Edwards, M. G. and Rogers, C. F.: 1998, Finite volume discretization with imposed flux continuity for the general tensor pressure equation, *Comp. Geosci.* **2**, 259–290.
- Edwards, M. G., Agut, R. and Aziz, K.: 1998, Quasi  $K$ -orthogonal streamline grids: gridding and discretization, paper SPE 49072 presented at the SPE Annual Technical Conference and Exhibition, New Orleans, September 27–30.
- Efendiev, Y. R.: 1999, The multiscale finite element method (MsFEM) and its applications, PhD Thesis, California Institute of Technology.
- Garcia, M. H., Journel, A. G. and Aziz, K.: 1992, Automatic grid generation for modeling reservoir heterogeneities, *SPE Res. Eng.* **7**, 278–284.
- Gomez-Hernandez, J. J. and Journel, A. G.: 1994, Stochastic characterization of grid block permeabilities, *SPE Form. Eval.* **9**, 93–99.
- He, C., Edwards, M. G. and Durlofsky, L. J.: 2002, Numerical calculation of equivalent cell permeability tensors for general quadrilateral control volumes, *Comp. Geosci.* **6**, 29–47.
- Hewett, T. A. and Yamada, T.: 1997, Theory for the semi-analytical calculation of oil recovery and effective relative permeabilities using streamtubes, *Adv. Water Resour.* **20**, 279–292.
- Holden, L. and Lia, O.: 1992, A tensor estimator for the homogenization of absolute permeability, *Transport in Porous Media* **8**, 37–46.
- Hou, T. Y. and Wu, X. H.: 1997, A multiscale finite element method for elliptic problems in composite materials and porous media, *J. Comp. Phys.* **134**, 169–189.
- King, M. J., MacDonald, D. G., Todd, S. P. and Leung, H.: 1998, Application of novel upscaling approaches to the Magnus and Andrew reservoirs, paper SPE 50643 presented at the SPE European Petroleum Conference, The Hague, The Netherlands, October 20–22.

- King, M. J. and Mansfield, M.: 1999, Flow simulation of geologic models, *SPE Res. Eval. Eng.* **2**, 351–367.
- Knupp, P.: 1995, Mesh generation using vector-fields, *J. Comp. Phys.* **119**, 142–148.
- Knupp, P.: 1996, Jacobian-weighted elliptic grid generation, *SIAM J. Sci. Comput.* **17**, 1475–1490.
- Lee, S. H., Durlafsky, L. J., Lough, M. F. and Chen, W. H.: 1998, Finite difference simulation of geologically complex reservoirs with tensor permeabilities, *SPE Res. Eval. Eng.* **1**, 567–574.
- Mao, S. and Journel, A. G.: 1998, Generation of a reference petrophysical/seismic data set: the Stanford V Reservoir, Stanford Center for Reservoir Forecasting Report.
- Portella, R. C. M. and Hewett, T. A.: 2000, Upscaling, gridding, and simulation using streamtubes, *SPEJ* **5**, 315–323.
- Prevost, M., Edwards, M. G. and Blunt, M. J.: 2001, Streamline tracing on curvilinear structured and unstructured grids, *SPEJ* **7**, 139–148.
- Renard, P. and de Marsily, G.: 1997, Calculating equivalent permeability: a review, *Adv. Water Resour.* **20**, 253–278.
- Ruge, J. W. and Stuben, K.: 1987, Algebraic multigrid (AMG), In: S. F. Mc Cormick (ed.), *Multigrid Methods. SIAM Front. Appl. Math.* **3**, 73–130.
- Tran, T. T.: 1995, Stochastic simulation of permeability fields and their scale up for flow modeling, PhD Thesis, Stanford University.
- Verma, S. and Aziz, K.: 1997, A control volume scheme for flexible grids in reservoir simulation, paper SPE 37999 presented at the SPE Reservoir Simulation Symposium, Dallas, June 8–11.
- Wallis, J. R., Kendall, R. P. and Little, T. E.: 1985, Constrained residual acceleration of conjugate residual method, paper SPE 13536 presented at the SPE Reservoir Simulation Symposium, Dallas, February 10–13.
- Wen, X. H. and Gomez-Hernandez, J. J.: 1996a, Selective upscaling of hydraulic conductivities, in: E. Baafi and N. Schofield (eds), *Geostatistics Wollongong '96*, Kluwer Academic Publishers, Dordrecht, The Netherlands, pp. 1112–1123.
- Wen, X. H. and Gomez-Hernandez, J. J.: 1996b, Upscaling hydraulic conductivities in heterogeneous media: an overview, *J. Hydrol.* **183**, ix–xxxii.
- Wen, X. H. and Gomez-Hernandez, J. J.: 1998, Upscaling hydraulic conductivities in cross-bedded formations, *Math. Geol.* **30**, 181–211.
- Wen, X. H., Durlafsky, L. J. and Edwards, M. G.: 2002, Improved upscaling of complex geological models on Cartesian grids, in review for *Math. Geol.*
- Wen, X. H., Durlafsky, L. J., Lee, S. H. and Edwards, M. G.: 2000, Full tensor upscaling of geologically complex reservoir descriptions, paper SPE 62928 presented at the SPE Annual Technical Conference and Exhibition, Dallas, October 1–4.